

MAKING ROOT CAUSE ANALYSIS FEASIBLE FOR LARGE CODE BASES: A SOLUTION APPROACH FOR A CLIMATE MODEL

PREPRINT, COMPILED FEBRUARY 12, 2019

Daniel J. Milroy
University of Colorado Boulder
daniel.milroy@colorado.edu

Allison H. Baker
National Center for Atmospheric Research
abaker@ucar.edu

Dorit M. Hammerling
National Center for Atmospheric Research
dorith@ucar.edu

Youngsung Kim
National Center for Atmospheric Research
youngsun@ucar.edu

Elizabeth R. Jessup
University of Colorado Boulder
elizabeth.jessup@colorado.edu

Thomas Hauser
University of Colorado Boulder
thomas.hauser@colorado.edu

ABSTRACT

Large-scale simulation codes that model complicated science and engineering applications typically have huge and complex code bases. For such simulation codes, where bit-for-bit comparisons are too restrictive, finding the source of statistically significant discrepancies (e.g., from a previous version, alternative hardware or supporting software stack) in output is non-trivial at best. Although there are many tools for program comprehension through debugging or slicing, few (if any) scale to a model as large as the Community Earth System Model (CESMTM), which consists of more than 1.5 million lines of Fortran code. Currently for the CESM, we can easily determine whether a discrepancy exists in the output using a by now well-established statistical consistency testing tool. However, this tool provides no information as to the possible cause of the detected discrepancy, leaving developers in a seemingly impossible (and frustrating) situation. Therefore, our aim in this work is to provide the tools to enable developers to trace a problem detected through the CESM output to its source. To this end, our strategy is to reduce the search space for the root cause(s) to a tractable size via a series of techniques that include creating a directed graph of internal CESM variables, extracting a subgraph (using a form of hybrid program slicing), partitioning into communities, and ranking nodes by centrality. Runtime variable sampling then becomes feasible in this reduced search space. We demonstrate the utility of this process on multiple examples of CESM simulation output by illustrating how sampling can be performed as part of an efficient parallel iterative refinement procedure to locate error sources, including sensitivity to CPU instructions. By providing CESM developers with tools to identify and understand the reason for statistically distinct output, we have positively impacted the CESM software development cycle and, in particular, its focus on quality assurance.

Keywords abstract syntax tree, program slicing, graph analysis, community detection, eigenvector centrality, root cause analysis

1 INTRODUCTION

The Community Earth System Model (CESMTM) is a commonly used application for simulating the climate system, and its influence extends from science to policy. The model's Fortran code base is modular, which facilitates its evolutionary and community development. The CESM has grown to approximately 1.5 million lines of code, which contain expressions of modern coding techniques together with code written in its earliest versions (decades ago). CESM's size, complexity, and continuous development make finding sources of error and value discrepancy difficult. While there are many debuggers capable of locating causes of runtime errors and segmentation faults in large-scale applications, there are few tools designed for root cause analysis of value discrepancies generated in large models (particularly those written in Fortran). We focus on the CESM in this work, though our root cause analysis methods may be applicable to other large Fortran models, or with a different parser, models written in other languages.

The first step to finding sources of inconsistency is to identify abnormal output. A simple test like bit-for-bit (BFB) equivalence is not useful because legitimate changes or optimizations

to the model can result in bitwise differences between outputs. The works [2, 3] establish statistical testing for consistency with an ensemble of "accepted" output from the Community Atmospheric Model (CAM) and Parallel Ocean Program (POP) component models of CESM. Ensemble methods are common in weather forecasting and climate studies; using them to test experimental outputs for consistency is broadly useful unlike simple BFB equivalence. The Ensemble Consistency Tests (ECTs) quantify the internal climate model variability present in an ensemble of the respective component models' outputs. The ECT then evaluates new, experimental outputs in the context of the ensemble to determine whether the new outputs are statistically consistent. The tests (together referred to as the CESM-ECT) provide an objective measure of difference without resorting to excessively strict metrics like BFB results. Moreover, the output of the tests does not require expert knowledge of climate science and returns a user-friendly *Pass* or *Fail*. The CESM-ECT has proven its value both in end-user testing and in port verification, where it was used to test CESM outputs from Cheyenne (the successor supercomputer) against the accepted ensemble generated on the Yellowstone supercomputer at the National Center for Atmospheric Research (NCAR).

While the CESM-ECT has been shown to work very well for correctly classifying new outputs, in the case of a failure it provides no information on the location or nature of the root causes. In fact, our work here is motivated by the need to provide this cru-

cial information, as its utility became apparent during our recent investigation into statistically distinct CESM output between two large supercomputers (detailed in [25]). Given CESM’s large and complicated Fortran code base, determining the reason for this CESM-ECT *Fail* required equal measures of data analysis, climate science knowledge, experience with the code base, and intuition. In all, we spent several months discovering the cause, and the process took the combined expertise of many scientists and engineers. Clearly, automating this process would be a tremendous asset for software engineers and scientists and would accelerate CESM development. In this work we make significant progress toward automating root cause analysis for sources of error and discrepancy in CESM, which is too large a model for direct application of currently available techniques.

This work is organized as follows. In Section 2, we overview our strategy and contributions and discuss related work. Section 3 describes identifying output variables most affected by inconsistencies. In Section 4, we detail transforming approximately 660,000 lines of code into a directed graph (digraph). In Section 5, we define our method of iterative convergence to locate sources of discrepancy, and in Section 6, we present examples of our method.

2 OVERVIEW AND RELATED WORK

In this section we provide a summary of the methods that we develop and describe our principal contributions. We then discuss related work on program slicing and runtime sampling.

2.1 Method and contributions

Here we overview our method and techniques for reducing the search space of possible causes of discrepancy. Recall that the process begins when CEST-ECT issues a *Fail*, indicating a statistical difference (or discrepancy) between the experimental output of interest and the accepted ensemble. We want to identify statistical differences as early as possible (i.e., at an early time step) in the simulation for several reasons: bugs or discrepancies may not propagate changes through the entire model, climate feedback mechanisms may not yet take effect, and less of the source code is executed. Therefore, we use the CESM-ECT tool that evaluates consistency at time step nine, which is called "ultra-fast" CAM-ECT, or UF-CAM-ECT [24].

A straightforward first step in reducing the search space is to eliminate modules that are not built into the final executable, and there may be many as CESM can be compiled with numerous configurations. Then, we use an existing code coverage tool to discard modules that are not yet executed by the second time step, as well as to remove unexecuted subprograms from the remaining modules. Next, we further reduce the scope by determining the CESM output variables (i.e., those written to file) that are most affected by the discrepancy, allowing us to disregard locations that compute other variables. In the commonly used CESM configuration that we use for our experiments in this work, these initial steps reduce the potential lines to search from about 1.5 million to 660,000, which is still substantial.

From this reduced code base, we construct a digraph of variable dependencies expressed through assignment statements. We then extract from this graph a subgraph that computes the

variables that we previously identified as most affected by the discrepancy. Next, to facilitate parallelism and runtime sampling (among other benefits that we describe later), we use clustering to partition the subgraph. For each cluster, we rank nodes based on their centrality to determine which code variables to sample at runtime accordingly. Finally, as a planned last step, we will further narrow the search space based on the runtime sampling results that indicate whether or not there are value differences between an ensemble and an experimental run, followed again by clustering and sampling by centrality to converge iteratively on the sources of discrepancy (currently performed in simulation). Figure 1 provides a schematic of our process.

While static program slicing, community detection, and centrality are well-studied and frequently used techniques in the areas of formal verification and graph analysis, to the best of our knowledge, their combination into a root cause analysis framework is novel. We make the following contributions in this work:

- We create a pipeline to convert the CESM source code into a digraph with extensive metadata that represents variable assignment paths.
- We develop a hybrid static program slicing approach that efficiently returns large slices.
- We devise an iterative refinement procedure based on community detection, centrality, and runtime sampling to contract the slice to a size amenable to analysis. Through community detection, the procedure can be performed in parallel.
- We perform experiments based on CESM output that demonstrate finding the causes of model discrepancy.
- We provide evidence that our methods accurately characterize information flow at runtime.

2.2 Related work

Program slicing is a common technique in debugging and in software development and maintenance that extracts sections of a program that can affect a particular region of code [38, 37]. In a broad sense, program slicing can be divided into two methods: static slicing, which considers all possible executions of a program, and dynamic slicing, which accounts for only one execution given a set of criteria (e.g., [36, 34]). Static slicing is generally less expensive but can return slices that contain too many extraneous statements to be useful [4]. Dynamic slicing can be far more precise but correspondingly expensive due to the inclusion of algorithms needed to evaluate the satisfiability of sections of the slice (such as SAT or Satisfiability Modulo Theory solvers [13]). So-called backward slicing considers subsets of code that affect a target location by backward traversal; it can be performed via static or dynamic slicing [18]. We are not aware of any dynamic slicing methods that can be applied to models consisting of over a million lines of code. We adopt the strategy of hybrid slicing [11], which uses dynamic information about program execution to refine static slices. In our case, the dynamic information is provided by a code coverage tool.

Program sampling or instrumentation provides detailed analysis of program states by monitoring variable values at runtime. This

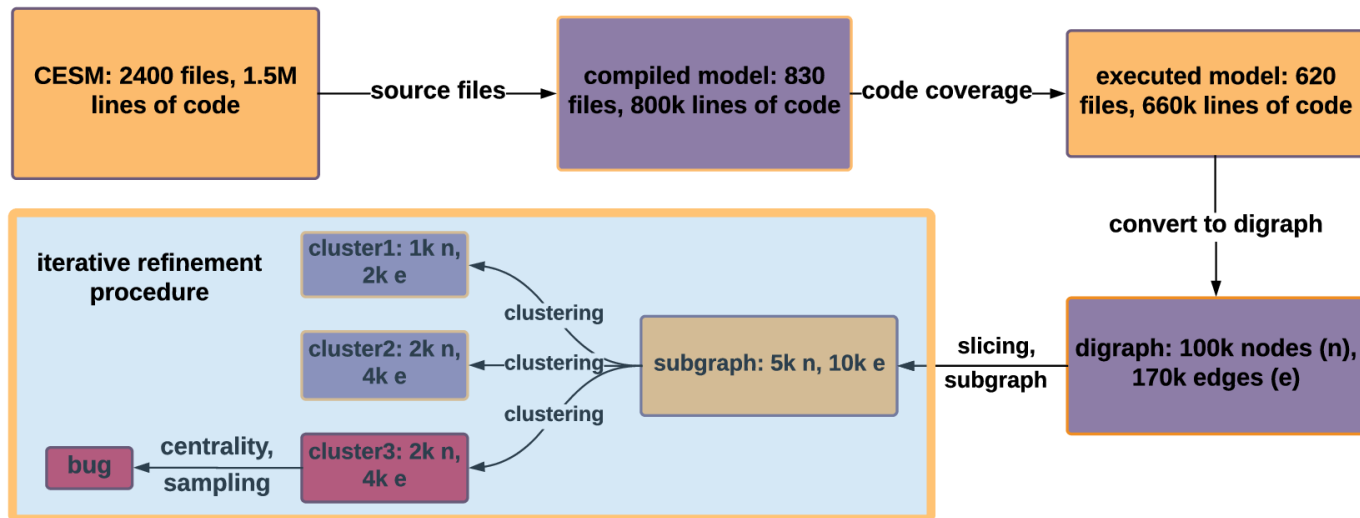


Figure 1: Process flow schematic of our methods.

type of monitoring can be used to detect divergent values of individual variables but can be extremely expensive (both in space and time) depending on the sampling frequency and the number of variables monitored. Many debuggers and profiling toolkits can perform sampling of large, distributed-memory applications (Allinea MAP and DDT [1], TotalView [35], and Tau [33], to name a few), and tools such as FLiT [31] and KGen [21, 20] can detect divergent values at runtime. We seek to reduce the search space of CESM to the point that such tools (or those of future design) can identify specific variables that cause model divergence.

3 IDENTIFYING AFFECTED OUTPUT VARIABLES

After UF-CAM-ECT returns a failure, our first step is to identify the CAM output variables that are affected (or most affected) by the cause of the failure. Doing so allows us to make a connection between the model outputs and the code itself. Ideally, we perform a straightforward normalized comparison of floating point values at the first model time step, selecting only those variables that exhibit a difference between a single ensemble member and a single experimental run. Because this approach is the direct measure of difference, we recommend using it first. However in our experience, it is most often the case that all CAM output variables are different at the model time step zero, so simply comparing floating point values is not useful for narrowing down the number of variables. Therefore, for these cases, we instead examine properties of the variables’ distributions with two variable selection methods to identify those most affected by the discrepancy.

The first method measures distances between the distribution medians of the ensemble and experimental runs for each variable. To make meaningful distance comparisons across variables, we standardize each variable’s distribution by its ensemble mean and standard deviation. Then we identify variables whose interquartile ranges (IQRs) of ensemble and experimental distributions do not overlap. We then rank these variables by descending order of distance between their medians. Although this provides a straightforward ordering of variables, the disadvantage of this

approach is that often many variables are identified. To be useful for tracing sources of inconsistency, the variable selection method should identify as few variables as possible (not more than 10). Our second method employs logistic regression with regularization via a penalized L_1 -norm (known as the lasso). We generate a set of experimental runs and use this in conjunction with our ensemble set to identify the variables that best classify the members of each set. We tune the regularization parameter to select about five variables as that yields a subset of CESM and CAM that, in our experiments, contains the known source of statistical inconsistency while still being small. The variables selected by the lasso (and their order) mostly coincide with the order produced by computing the distance between standardized medians.

CESM and CAM present a challenge for variable selection techniques, as the models’ interconnectivity results in most changes (in software or hardware) propagating through the atmosphere model rapidly, and affecting most variables. Since many of the experiments in this work represent modifications to code present in the tightly connected “core” of CAM, it is reasonable that variable selection is difficult. Variable selection for smaller or simpler models may represent less of a challenge.

4 FROM SOURCE CODE TO DIGRAPH

Finding lines of code that modify a particular CAM output variable seems a straightforward task: use a text-based search to select code that modifies the variable in question. However, many internal variables may alter values that eventually propagate to the affected output values, and the data dependencies are likely to be complicated. To describe the relationships between CESM variables accurately, we convert each source code file into an Abstract Syntax Tree (AST), which represents code syntax as structural elements of a tree. From the ASTs we create a digraph which represents variable dependencies. Figure 2 provides a simple example of the transformation of source code assignments to a digraph.

4.1 Generating the AST

To construct the AST for CESM, we need to parse the source code. We use the same CESM version as in [19], and our experimental setup (FC5) consists of a subset of all available component models. Before parsing, we do several preprocessing steps to exclude code that is not executed. Unfortunately, the CESM build system obfuscates which components’ Fortran modules are compiled into the specified model. Therefore, we employ KGen [21, 20], a tool to extract and run code kernels as standalone executables, to identify the files compiled into the executable model, reducing the number of modules from approximately 2400 to the nearly 820 used by our experimental setup. KGen also replaces preprocessor directives with their compile-time values, enabling conversion of Fortran code to a Python AST via fparser (based on F2PY [28]). Fparser is the only tool that we are aware of to parse Fortran into Python data structures.

We further limit the scope of code considered by examining coverage, which identifies code lines, subprograms, and modules executed in a given application. Since our objective is to identify critical code sections as early as possible in the CESM runtime, we can ignore many subsections of code which are not yet run. To find such code, Intel provides a code coverage tool [17] that writes profiling files that indicate coverage down to individual lines. In our experience, the tool returns accurate evaluations to the level of subprograms, but its behavior at the line-level is inconsistent. Nevertheless, finding entire unused modules and uncalled subprograms is useful and reduces the number of modules and subprograms to be parsed by about 30% and 60%, respectively. We develop software to parse the codecov HTML output, using the output to remove unnecessary modules and comment out unused subprograms.

4.2 From AST to digraph

After converting each Fortran module file into an AST, we extract data dependencies to form a digraph. See Figure 3 for a visual overview. We need to resolve all assignments, as directed paths of assignments define dependencies between variables. Tracing dependencies between subprograms (similar to interprocedural program slicing [37]) requires processing subroutine and function calls, interfaces, use statements, etc. Assignments without functions or arrays are processed immediately. To allow correct mappings between call and subprogram arguments, parsing statements with calls must be done after all source files are read. Furthermore, Fortran syntax does not always distinguish function calls from arrays, so correct associations must be made after creating a hash table of function names.

Transforming the CESM source code into a digraph presents several challenges. Fparser sometimes fails to convert a Fortran file into an AST due to bugs and statements that exceed fparser’s capabilities (e.g., one CESM file contains a statement with more than 3500 characters). In fact, CESM contains thousands of expressions that are highly complex, with deep function and subroutine calls. Because existing Fortran parsing tools are inadequate for CESM, we employ three different parsers for each assignment (some are subjected to multiple passes of these parsers): fparser, KGen helper functions, and a custom string parsing tool based on regular expressions and Python string

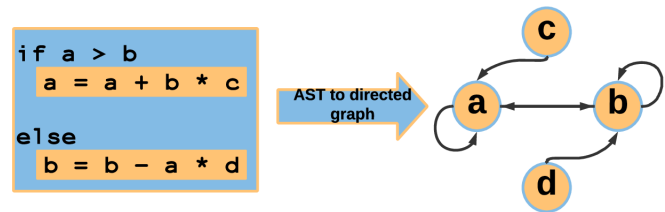


Figure 2: Example statement as source code and its directed graph representation.

manipulations that we developed to process cases unhandled by the other tools.

Processing the ASTs results in a *metagraph* Python class that contains a digraph of internal variables, subprograms, and methods to analyze these structures. CESM internal variables are nodes with metadata, such as location (module, subprogram and line) and “canonical name” (the variable name before being entered into the digraph - which requires unique node names). The digraph component of the metagraph is a NetworkX digraph [12]. NetworkX is a Python graph library that provides an extensive collection of easy to implement graph algorithms and analysis tools.

Note that with static analysis it is not always possible to determine which function a Fortran interface call actually executes at runtime. Therefore, we adopt the conservative approach of mapping all possible connections. We map the target of “use” statements to their local names to establish correct local symbols for remote procedures, resolving Fortran renames. If the use statement does not specify an “only list,” then we map all public variables in the source module to their target module variables. We do not consider chained use statements (i.e., where module A uses B, which uses C), since accurate dependency paths can be created by connecting the statements independently.

With these associations defined, we iterate through statements containing subroutine calls and possible functions or arrays. We process subroutine and function calls by treating each argument as a tree, and we successively map outputs of lower levels to corresponding inputs above. Each output gets an edge to the above layer’s input, which injects the call’s graph structure into the CESM digraph. The top level argument output is connected to the subroutine’s corresponding argument in its definition. Discerning functions from arrays is addressed by hash table lookups in the metagraph. Ultimately, the expression’s right-hand-side variables and arrays and function (or subroutine argument) outputs are given edges to the left-hand-side. We process Fortran intrinsic procedures like `min` or `max` by creating paths from their inputs to themselves, and then to their outputs. We localize the intrinsic procedures to the line of code where they are called (i.e. a unique name like `min_100_modname`) to avoid creating spurious, highly connected variables. An example of node-edge mapping within a composite function is provided by the following process, where each function’s internal variables form a path connecting its inputs to its outputs, in order of depth:

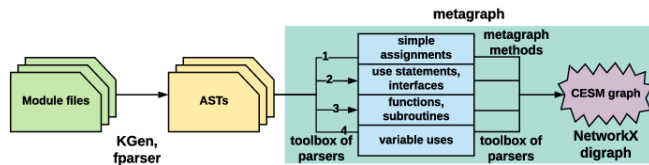


Figure 3: Converting Fortran files into a metagraph.

$$\begin{aligned} \omega &= \alpha(b(c, d) * e(f(g + h))) \\ h &\rightarrow \text{input}(f) \\ g &\rightarrow \text{input}(f) \\ \text{output}(f) &\rightarrow \text{input}(e) \\ c &\rightarrow \text{input1}(b) \\ d &\rightarrow \text{input2}(b) \\ \text{output}(e) &\rightarrow \text{input}(\alpha) \\ \text{output}(b) &\rightarrow \text{input}(\alpha) \\ \text{output}(\alpha) &\rightarrow \omega \end{aligned}$$

We adopt a conservative approach for handling composite and complex Fortran data structures. Arrays are considered atomic in that we ignore indices. Pointers are treated as normal variables. Fortran derived types are challenging, as they can be chained into deep composite data structures. We define the indexed element of the derived type as the metagraph canonical name, e.g., `elem(ie) %derived %omega_p` has a canonical name of “omega_p.” In effect, we are compiling the CESM Fortran source code into node relationships in a digraph. Note that our parsing process is able to handle all but 10 assignment statements of the 660,000 lines of code in the coverage-filtered source.

While details such as subroutine call handling, use statements, and derived types are specific to Fortran, the overall approach of converting source code to a directed graph can be accomplished with any compiled language. In particular, the LLVM compiler infrastructure project [22] features the Clang language front-end for C language family (C++, Objective C/C++, OpenCL, CUDA, and RenderScript) codes [16]. When generating an intermediate representation of supported C language family code, Clang creates an AST with a convenient API (libclang). The libclang API provides Python bindings which permit AST traversal and source-AST mappings that can be used similarly to Fparser. We can adapt our Python software to traverse and convert the Clang AST to a directed graph for C/C++ codes as well. Modifying our project to enable analysis of C family codes is future work.

5 ANALYZING THE CESM GRAPH

At this point, we have transformed the CESM code into a digraph that is composed of nodes, which are variables present in assignment expressions, and directed edges that indicate the directionality of the effect of one variable upon another. Now we narrow the scope of our search for the source of the discrepancy by analyzing the graph, usually accomplished by program slicing. Static slicing often produces slices that are too

large to locate error sources, and dynamic slicing, while more precise, is too expensive to apply to the CESM graph (about 100,000 nodes and 170,000 edges). Therefore, to make locating internal CESM variables or nodes that influence the values of the affected output variables more tractable, we examine static data dependency paths that terminate on these variables. We mitigate the imprecision of static backward slicing by integrating graph analysis algorithms to refine our slices. In this section, we discuss these methods and propose an iterative subgraph refinement procedure that involves runtime sampling of CESM nodes.

5.1 Tracing affected internal variables

Since variable relationships in assignment statements are represented as directed edges in the graph, we are interested in directed paths through CESM. These paths ignore control flow such as “if” statements or “do loops,” so this approach is akin to backward static slicing. A key difference between our approach and typical program slicing is that nodes in the graph are single variables rather than expressions of multiple variables. Slicing criteria are thus single variables. When used in conjunction with runtime information in the form of code coverage, our method can be considered a type of hybrid slicing (e.g., [11]).

In NetworkX, the fastest way to determine dependencies is by computing shortest paths. In particular, we seek the shortest paths that terminate on a CESM output variable. Unfortunately, finding the output variables in CESM is a challenge in its own right. Ideally, we would find the locations where I/O calls are made with the output variables as arguments, and then find all shortest paths in the graph that end on those calls. Considering these paths does not work well in practice because CESM subprograms that write derived types, e.g., `state%omega`, usually take the base derived type (`state`) as an argument, rather than the derived type element (`omega`). This means that there are few paths that terminate on `state%omega` at the call location. We address this problem by searching for paths that terminate on nodes with the canonical name (see Section 4) of `omega`. This approach increases the size of our static slice, but with the attendant advantage that the discrepancy source will very likely be contained in the slice.

CESM I/O statements use temporary variables extensively and include character type variables in the output name argument, so uncovering the exact variable output for a given I/O call must be done with custom instrumentation. Of the nearly 1200 CAM I/O calls which write output variables, many include variables to label the output. To resolve these variables, we instrument the code to print the corresponding string label, permitting a mapping between internal variable names and names written to file. For example, we do not search for paths that end on CAM output flds, but on variables whose canonical names are the internal name `fldws`.

So given a set of output variables that are affected by a certain change (determined as described in Section 3), we compute the shortest directed paths that terminate on these variables with Breadth First Search (BFS). After finding these paths, we form the union of the node sets of all such paths. We are interested in the union rather than the intersection as multiple disjoint code sections can be involved in the computation of an affected

variable. Such a scenario can arise when conditionals dictate whether I/O calls are executed. Using the union of all shortest paths terminating on the internal canonical names of affected output variables, we induce a subgraph on CESM, which yields the graph containing the causes of discrepancy.

5.2 Community structure and node centrality

Since CESM and its component models are modular, it is reasonable to conclude that its graph should exhibit clusters corresponding to the modules or related processes. Induced subgraphs of CESM may contain cluster or community structure that can be exploited to improve our root cause search, which ends with sampling affected variables. Since sampling can be an expensive process, only a limited number of nodes in the subgraph should be instrumented. By partitioning the subgraph through community detection, we can choose a small number of highly connected nodes in each community to sample and perform the instrumentation of these nodes independently (in parallel). This process can be performed iteratively to reduce the search space.

CAM contains two main processes: physics (sub-grid scale) and dynamics, which taken together feature a set of highly connected modules (the “core”). These CAM modules are involved in the computation of many of the output variables, and the sources of the discrepancy (which we will also refer to as “bugs” for simplicity) are likely to affect multiple output variables. An examination of node connectivity in the core reveals clustering of highly connected nodes in different communities. Although sampling the whole core’s most connected nodes may detect floating point differences between ensemble and experimental runs, instrumenting highly connected nodes in each community instead can reduce the distance between instrumented variables and bug locations (reducing the number of iterations needed to refine the search space).

Centrality is a fundamental way to distinguish nodes in a graph. Two simple examples of centrality are degree centrality, which counts the number of edges connected to a given node, and betweenness centrality, which counts the number of BFS or Dijkstra shortest paths (for weighted graphs) that traverse a node (or edge). Graph analysis via centralities proves useful in many diverse areas of research, e.g., [9, 30, 32, 5]. A study of the relationship between brain regions’ centralities and physical and cognitive function [15] is particularly relevant to our work. They conclude that such analysis consistently identifies structural hubs (high centrality regions) in the cerebral cortex, and that “high centrality makes hubs susceptible to disconnection and dysfunction.”

The Girvan-Newman algorithm (G-N) [10, 26] is a popular method for identifying communities in undirected graphs. The algorithm is based on edge betweenness centrality, which ranks edges by the number of shortest paths (computed via BFS) that traverse them. The algorithm successively removes the edge with highest centrality in each connected component, which breaks the graph into ever smaller communities. G-N identifies communities via the following steps [10]:

1. calculate the betweenness for all edges in the network
2. remove the edge with the highest betweenness
3. recalculate betweenness for all edges affected by the removal

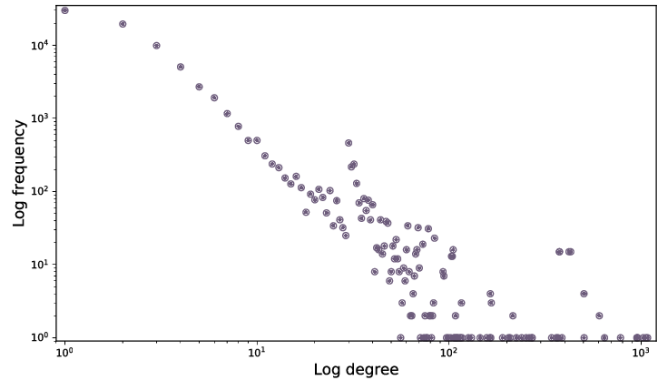


Figure 4: Degree distribution of nodes in the CESM digraph.

4. repeat from step 2 until no edges remain

In practice each iteration involves removing the edge with the highest betweenness until the number of communities increases [26]. Note that G-N was formulated to identify communities in undirected graphs. In our case, we convert the directed subgraph into an undirected subgraph for purposes of community detection. This conversion is desirable for our work, as it is equivalent to forming the weakly connected graph of the directed subgraph. Weakly connected graphs are digraphs where any node can be reached from any other node by traversing edges in either direction. Bug locations may be anywhere in the subgraph, so we cannot impose assumptions about whether instrumented nodes are reachable via bug sources in the digraph (even between communities) in either direction. However, in our experiments (presented in Section 6), we know where the bug locations are, so we can simulate how our sampling procedure detects floating point differences between the ensemble and experiment. Given our knowledge of directed paths’ connectivity from known bug sources to central nodes, we can deduce whether a difference can be detected. For our method to be useful in situations where bug locations are unknown, we cannot assume such knowledge when we identify communities.

5.3 Finding important nodes with centrality

Given a modification that alters the values of a set of output variables, we seek locations in CESM that influence their computation. The CESM digraph lacks any information about the nature of connections between variables, so, for example, linear and exponential relationships are expressed identically in the graph. Indeed, the connectivity of the CESM graph is the only information we have to identify important locations in the code for sampling.

We use centrality to select nodes whose values are likely to be affected by the causes of statistical distinguishability. We can then sample the variables’ runtime values to detect differences between an experimental and a control (or ensemble) run. Eigenvector centrality is a promising choice, as it considers not only the degree of each node, but the degrees of its neighbors and their neighbors, and is related to information flow in a graph. In fact, eigenvector centrality is related to PageRank, which is used to rank web pages in search results [27]. In this work we focus on in-centrality, as we seek nodes which are likely to be affected by the bug sources. From the perspective of sam-

pling, we are looking for information sinks rather than sources. Eigenvector centrality has the disadvantage of favoring hubs (highly connected nodes), which “causes most of the weight of the centrality to concentrate on a small number of nodes in the network” for power law graphs [23]. The degree distribution of the total CESM graph approximately follows a power law, as can be seen in Figure 4. Induced subgraphs of the CESM graph are also plausibly scale-free. A natural question is whether the concentration of centrality on graph hubs has undesirable effects on the ranking of nodes. We found that the application of non-backtracking centrality (based on the Hashimoto matrix [14]) provides no advantage over standard eigenvector centrality for the CESM graph, its subgraphs, or communities. However, it may prove beneficial for models with graphs that follow a power law that produce more pronounced localization [23].

5.4 Iterative refinement procedure

Once communities are detected in the subgraph, we compute each community’s eigenvector in-centralities and choose the top nodes to sample. The number of nodes to sample is dictated by available computational resources. Based on whether a value difference can be found between the nodes sampled in the ensemble run and the experimental run, we can iteratively reduce the size of the subgraph to converge on the sources of statistical inconsistency. This iterative approach is similar to a k -ary search, which is a generalization of binary search. In binary search, the search space is halved and a single determination is made at each iteration, however for k -ary search the space is partitioned into k sections and k evaluations are made at each iteration. In our case k varies by iteration depending on the number of communities identified. The following algorithm summarizes our overall approach:

Algorithm 5.4

1. Perform variable selection detailed in Section 3
2. Map the set of affected CAM output variables in step 1 to their internal CAM variables $\{V_i\}$
3. For each affected internal variable V_i , use BFS to find the set of nodes $\{n_i\}$ in all shortest paths that terminate on variables with canonical names equal to V_i in the CESM digraph
4. Form the induced subgraph G via the union of nodes in the paths in step 3
5. Use G-N to identify the communities $\{C_k\}$ of undirected G (omitting communities smaller than 3 nodes)
6. Compute the eigenvector in-centrality for each C_k and select m nodes with largest centrality $\{n_{k_i}\}$
7. Instrument $\{n_{k_i}\}$ for all k in parallel for an ensemble run and an experimental run, noting the set of nodes which take different values $\{d_{k_i}\}$ ($\{d_{k_i}\} \subseteq \{n_{k_i}\}$)
8. (a) If $\{d_{k_i}\} = \emptyset$ (i.e., no different values are detected), form the induced subgraph on all nodes in G that are not in BFS shortest paths that terminate on $\{n_{k_i}\}$
 (b) Else, form the induced subgraph of G generated by nodes in G that belong to BFS shortest paths that terminate on $\{d_{k_i}\}$

9. Repeat steps 5-8 until the subgraph is small enough for manual analysis or the bug locations are instrumented

There are three issues involved in the process above that merit discussion. First, it is possible that steps 5-8b in algorithm 5.4 do not refine the subgraph of the previous iteration (i.e., if the subgraph connectivity is such that all nodes are connected to all central nodes that take different values between the ensemble and experimental runs). In this case, we can select a subset of the most central nodes “most affected” by the bugs. The second issue is that it is possible that the bug sources are not contained in any community i.e., if a bug is in an output variable that has only one neighbor. In this case, no different values will be detected in step 7, and the new induced subgraph will still meet the condition in step 8a. The next iterations will not detect differences, and the successive subgraphs will become increasingly disconnected. Eventually G-N will not identify any communities, and the resulting nodes will need to be analyzed. The third issue is an artifact of static slicing: since the paths do not take into account, e.g., conditional branches, some of the paths may not be traversed. We need to develop a method to track edge traversal and remove invalid paths; algorithm 5.4 must only remove nodes that actually can influence $\{n_{k_i}\}$ in step 8a.

Unless otherwise noted, we perform only one iteration of G-N in algorithm 5.4 step 5. We could use a larger number to further subdivide the induced subgraph in each iteration (possibly enabling more parallelism), but we adopt a conservative approach to avoid clustering the subgraphs far beyond the natural structure present in the code. Note that excessive G-N iterations would not prevent algorithm 5.4 from locating bug sources, but it can slow the process.

6 EXPERIMENTS

We apply the overall method discussed in Section 5.4 to six experiments, and for the sake of brevity present four examples in detail. For all but one experiment, we introduce a bug into the source code so that the correct location is known. We then verify that our method can be used to identify the bug location in CESM by demonstrating how it would converge on the location given instrumentation. We first show that our method can correctly identify straightforward single-line bugs before proceeding to more complicated sources of output discrepancy, such as the identification of variables most affected by certain CPU instructions. We make the following choices and assumptions in our experiments (unless otherwise noted): we restrict our subgraphs to nodes in CAM modules, perform a single G-N iteration (within algorithm 5.4 step 5), choose the top 10 nodes by in-centrality to sample, and assume all paths are traversed at runtime. We restrict our experiments here to graph nodes from CAM modules as this reduces the number of iterations required and simplifies the graphs that we present. We note that we have successfully located bugs in the land module as well. Restricting nodes to CAM disconnects paths with segments in other component models, producing residual clusters of less than four nodes that are separated from the main communities. We remove these small clusters for the sake of clarity in our plots; their removal does not affect the results.

In the figures that follow, subfigures **a** are the outputs of algorithm 5.4 step 4, 8a, or 8b, depending on the iteration or whether simulated sampling detects differences. Subfigures **b** color members of each community detected by step 5, and subfigures **c** represent the output of step 7 for the community containing the discrepancy sources. Each of the following subsections describes a different experiment. Since we are unaware of methods capable of analyzing models as large as CAM or CESM, we do not perform comparisons with existing techniques.

6.1 *WSUBBUG*

We begin our testing with a bug in an isolated CAM output variable: `wsub`. By isolated we mean disconnected from the CAM core (see Section 5.2) and highly localized. Such a bug has minimal effect and scope which is a good sanity check for our method. The bug consists of a plausible typo (transposing 0.20 to 2.00) in one assignment of `wsub` in `microp_aero.F90`. The variable is written to file in the next line, so this bug affects only the single output variable. This small change produces a UF-CAM-ECT failure. In this case the median-distance method clearly indicates that the `wsub` variable is distinct; the distance between the experimental and ensemble medians for this variable is more than 1,000 times greater than for the variable ranked second. The induced subgraph contains only 14 internal variables, all of which are related to `wsub`, with one being the bug itself.

6.2 *RAND-MT*

This example, *RAND-MT*, involves replacing the CESM default pseudorandom number generator (PRNG) with the Mersenne Twister. This experiment appears in [24] as an example that results in a UF-CAM-ECT failure. The random number generator is used to calculate distributions of cloud-related CAM variables, and this experiment is interesting because it is not a bug (in the usual sense of being incorrect) and not localized to a single line. We identify the variables immediately influenced or defined by the numbers returned from the PRNG, and consider them to be the bug locations. The lasso variable selection method identifies the five output variables most affected by the PRNG substitution. From these variables, we extract a subgraph of 4,509 nodes and 9,498 edges. Given the size of this induced subgraph, we must use our iterative technique on subgraph communities to reduce the scope of our search. G-N identifies two main communities (blue and green in Fig. 5b) in the CAM core. The smaller, green community contains the nodes computed using output from the PRNG. Instrumenting the top 10 most central variables in this community would not detect a difference, as there are no paths from the variables in the bug location to these nodes (see Fig. 5c). Executing algorithm 5.4 step 8a admits a dramatic reduction in the search space (Figure 6a). Instrumenting the most central, orange nodes in Figure 6c would indicate a difference as there are multiple paths from the discrepancy sources. This subgraph is small, and the sources are sufficiently near the sampling sites that the cause could be found at this stage.

It is noteworthy that the induced subgraph does not contain all the source locations of the statistical distinguishability. The PRNG in CAM is called in two modules: one that computes cloud cover given longwave radiation, and the second with shortwave radiation. The combination of `f1wds` (downwelling long-

wave flux at surface) and `qr1` (longwave heating rate) causes the longwave module to be present in the induced subgraph. However, the two variables that are needed to include shortwave radiation in the induced subgraph (`fsds` and `qrs`) are not in the set of first five variables returned by lasso. The difficulty in selecting a set of variables that can be traced exactly to the regions of code responsible for statistical inconsistency means that some code sections can be omitted. However, the fact that many variables are computed in common regions of code that are interconnected graphically means that our method will identify many of these regions.

This experiment highlights an important advantage of community detection, namely that it separates tightly connected clusters and exposes smaller clusters within communities whose nodes dominate the centrality of the entire subgraph (see Section 5.2). If we were to sample the most central nodes of the entire subgraph (without considering communities) in Figure 5a, we would be concentrating on the centrality-dominant blue community, and it could take many iterations of sampling blue community nodes to reach nodes in the green community.

6.3 *GOFFGRATCH*

Our third experiment is a modification in the Goff and Gratch Saturation Vapor Pressure elemental function. We change a coefficient of the water boiling temperature from $8.1328e-3$ to $8.1828e-3$. This easy to miss typo results in a UF-CAM-ECT failure. The output of the Goff and Gratch function is used extensively in the CAM core, so its effects are not localized.

For this experiment, we note that the lasso variable selection method selects 10 variables (instead of 5). Due to experiment-specific conditions, tuning the regularization parameter to select only five variables would require a more sophisticated approach. Inducing a subgraph on locations that compute these 10 variables results in a graph of 4,243 nodes and 9,150 edges (Figure 7a). Note that the largest community (blue in Figure 7b) contains the nodes affected by the incorrect coefficient. Instrumenting the top 10 most central variables in this community would detect a difference, as there are paths from the bug locations to these nodes (Figure 7c).

For the second iteration, inducing a new subgraph of all shortest paths terminating on the central nodes in Figure 7c (algorithm 5.4 step 8b) returns a subgraph that includes part of the green community from the first iteration. Subsequent community detection reveals the remnants of the green community of the first iteration, which are then excluded by sampling. However, in this case, no further simulated iterative refinement can be performed by inducing a subgraph on nodes connected to the instrumented variables, as this subgraph is so highly connected that the induced subgraph equals the community subgraph (nearly identical to Figure 7c). We omit plots of the second iteration due to similarity with Figure 7.

To refine the blue community from Figure 7c we need to handle the case where the induced subgraph does not refine the subgraph from the previous iteration. In future work we can rank the differences obtained by sampling and further refine the subgraph based on the nodes with the greatest differences. Alternatively, if we learn that all nodes are affected equally, we can choose one node and induce a subgraph based on paths terminating

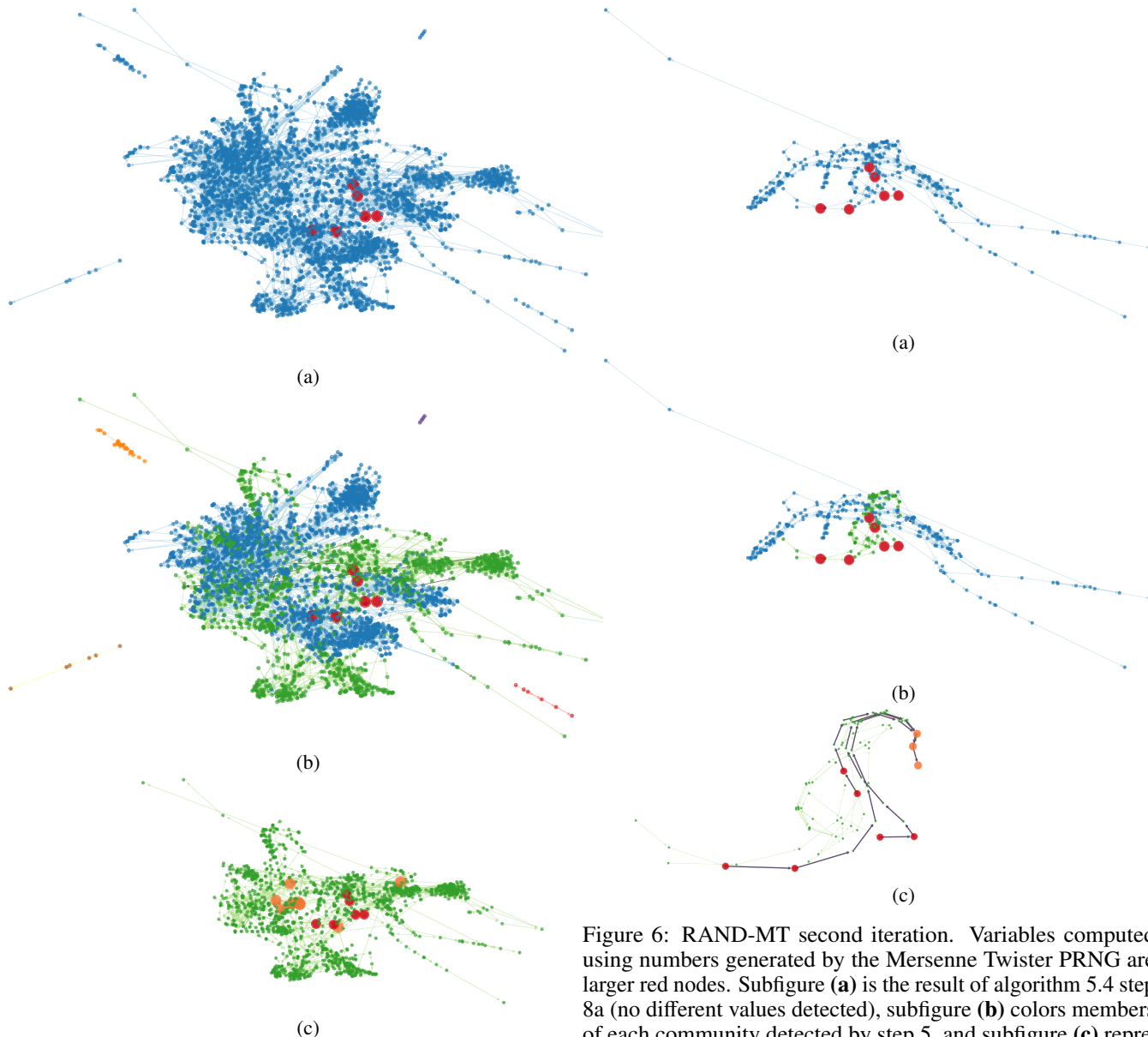


Figure 5: RAND-MT first iteration. Variables computed using numbers generated by the Mersenne Twister PRNG are larger red nodes. Subfigure (a) is the result of algorithm 5.4 step 4, subfigure (b) colors members of each community detected by step 5, and subfigure (c) represents the output of step 7 for the community containing the bugs. Larger orange nodes in subfigure (c) indicate those with the largest eigenvector in-centrality.

on it. There are numerous algorithms for graph partitioning which we could use in conjunction with sampling in the case of GOFFGRATCH, and there are many options to test when we realize our process with sampled data (which is also future work). The power of our graphical method is that it enables diverse types of graph analysis.

Figure 6: RAND-MT second iteration. Variables computed using numbers generated by the Mersenne Twister PRNG are larger red nodes. Subfigure (a) is the result of algorithm 5.4 step 8a (no different values detected), subfigure (b) colors members of each community detected by step 5, and subfigure (c) represents the output of step 7 for the community containing the bugs. Larger orange nodes indicate those with the largest eigenvector in-centrality that can be sampled at runtime. We choose three here given the small size of the subgraph.

6.4 AVX2

As noted in Section 1, our work here to develop an automated process was motivated by our investigation in [25] to find the cause of the CESM-ECT failure on the Mira supercomputer [8] when compared to the ensemble from NCAR’s Yellowstone machine [7]. To summarize briefly, the manual process in [25] included measuring each CAM output variable’s contribution to the CAM-ECT failure rate, which identified the most affected output variables. We were then able to determine that computations in the Morrison-Gettleman microphysics module (MG1) were problematic [25], and, with the previously mentioned KGen tool [21, 20], convert the MG1 module into a kernel. In the MG1 kernel, we found variables which had substantially

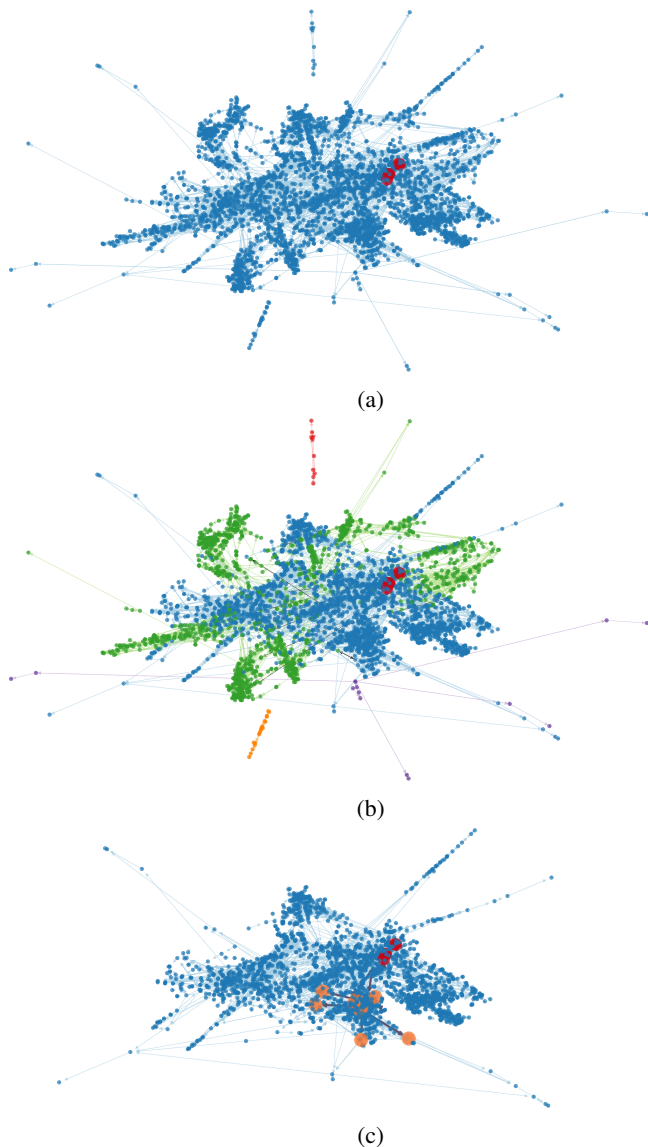


Figure 7: GOFFGRATCH, first iteration. Subfigure (a) is the result of algorithm 5.4 step 4, subfigure (b) colors members of each community detected by step 5, and subfigure (c) represents the output of step 7 for the community containing the bugs. The bug locations are indicated as large red nodes, and the top 10 most central variables in the blue (physics) community are indicated by larger orange nodes. Path segments from the bugs to the sampled central nodes are thicker purple edges.

different values between Yellowstone and Mira and were able to attribute the difference to Mira’s FMA instructions. We note (for later comparison) that one of these variables was `nctend`, which is modified by a frequently used temporary variable `dum` and that `nctend` also exhibits significantly different values between Yellowstone and Haswell generation (FMA capable) Intel CPUs (i.e., the FMA discrepancy is not limited to Mira). In this section, we demonstrate our automated method could obtain these same results that took several months and many CESM experts.

Because we are no longer able to use Mira and Yellowstone, we instead evaluate the impact of FMA on the newer Cheyenne

machine [6]. Cheyenne contains Intel Broadwell CPUs, which support the Intel AVX2 instruction set, and these instructions include FMA. For this work, we compare an ensemble generated with AVX2 disabled (thus disabling FMA) to an experimental set generated with AVX2 (and FMA) instructions enabled. We verify that enabling AVX2 and FMA causes a UF-CAM-ECT failure (see Table 1). Since FMA instructions can be generated from many different lines of source code (distributed sources of discrepancy), we employ KGen to identify a small number of variables affected by AVX2 and FMA to designate as bugs. We extract the Morrison-Gottelman microphysics kernel identified in [25] and compare the normalized Root Mean Squared (RMS) values computed by the kernel with AVX2 disabled to the normalized RMS values with AVX2 enabled. KGen flags 42 variables as exhibiting normalized RMS value differences exceeding 10^{-12} . Here, we determine if our iterative refinement procedure can find some of these variables given CAM outputs most affected by AVX2 instructions.

Inducing a subgraph on assignment paths that compute CAM output variables affected by enabling AVX2 instructions (selected by lasso) results in the graph in Figure 8a (4,159 nodes and 9,028 edges). Five of the 42 variables identified by KGen are present in this subgraph, all of which are in the blue community of Figure 8b. This community contains the CAM core physics processes, of which MG1 forms a central part. The node with the largest eigenvector in-centrality is the temporary, dummy variable `dum` in Figure 8c. Four of the five variables with normalized RMS values exceeding our threshold are in the top 15 nodes with the greatest in-centrality. These variables are `nctend`, `qvlat`, `tlat`, and `nitend`. The fifth variable, (`qsout`), is modified by `qniic` (in the top 15 most central nodes) in an assignment statement. All five variables have paths that terminate on all 15 most central nodes. The following Python REPL output lists the nodes in the blue community of Figure 8c in descending order of their eigenvector in-centrality values. Each ordered pair contains a node name and a centrality value. The node name includes a suffix demarcated by a double underscore; this suffix indicates the subprogram containing the variable (here the `micro_mg_tend` subroutine in the Morrison-Gottelman microphysics kernel) to guarantee unique names in the directed graph (see Section 4.2). Node names colored red are those exhibiting values exceeding our normalized RMS threshold.

```
>> avx2_bluecommunity_incentrality[:16]
(dum_micro_mg_tend, 0.455153),
(ratio_micro_mg_tend, 0.325264),
(tlat_micro_mg_tend, 0.255383),
(qniic_micro_mg_tend, 0.198578),
(nric_micro_mg_tend, 0.196431),
(nsic_micro_mg_tend, 0.191075),
(qctend_micro_mg_tend, 0.188477),
(qric_micro_mg_tend, 0.180318),
(qitend_micro_mg_tend, 0.15969),
(prds_micro_mg_tend, 0.157626),
(pre_micro_mg_tend, 0.157551),
(nctend_micro_mg_tend, 0.148088),
(qvlat_micro_mg_tend, 0.132584),
(mnucc_micro_mg_tend, 0.121525),
(nitend_micro_mg_tend, 0.120172),
(nsagg_micro_mg_tend, 0.109382)
```

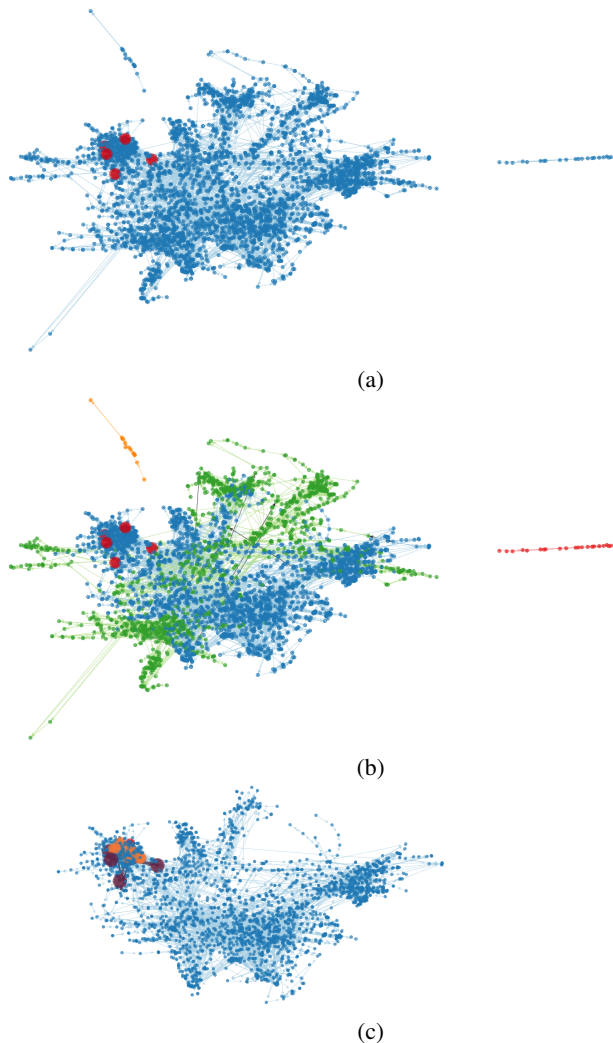


Figure 8: AVX2. Variables found to take significantly different normalized RMS values between Broadwell CPUs with AVX2 enabled (FMA enabled) and AVX2 disabled (FMA disabled) are larger red nodes (`nctend`, `qvlat`, `tlat`, `nitend`, and `qsout` in MG1) and also in the top 15 most central nodes. Large orange nodes are remaining nodes in the top 15. Subfigure (a) is the result of algorithm 5.4 step 4, subfigure (b) colors members of each community detected by step 5, and subfigure (c) represents the output of step 7 for the community containing the bugs. Bugs detected by sampling are colored purple.

That our iterative refinement procedure would sample and identify the locations of nodes known to be most affected by AVX2 instructions on the first iteration is a testament to the potential utility of our method, particularly in the challenging case where hardware or CPU instructions cause statistical distinguishability.

6.5 AVX2 in the CESM graph

Here, we deviate slightly to discuss how centrality can be used to identify Fortran modules crucial to information flow in the overall CESM graph. While the MG1 module and its constituent variables are causes of ECT failure with AVX2 and FMA enabled, these instructions can be generated in many CESM mod-

Table 1: Selective AVX2 disablement

Experiment	ECT failure rate
AVX2 enabled, all modules	92%
AVX2 disabled, 50 largest modules	86%
AVX2 disabled, 50 rand mods (10 sample avg)	83%
AVX2 disabled, 50 central modules	8%
AVX2 disabled, all modules	2%

ules. This suggests we compute the (in and out) centrality of the modules themselves (rather than individual variables) to rank them by their potential to propagate FMA-caused differences within CESM. This viewpoint applies to other machine instructions or hardware errors.

To calculate the centrality, we must collapse the graph of variables into modules by considering the graph minor of CESM code formed by the quotient graph of Fortran modules. A graph minor is a subgraph of a graph G obtained by contracting edges of G . This graph minor identifies (or collapses) nodes using an equivalence relation, meaning that if two nodes satisfy the equivalence relation, they are replaced by a single node. Edges between equivalent nodes are deleted, and edges between remaining nodes and the new node are preserved. In this case we use the equivalence relation $v_1 \sim v_2 \iff v_1$ and v_2 are in the same CESM module (modules become equivalence classes). Applying this equivalence relation to the CESM graph yields a digraph of 561 nodes and 4,245 edges. Selectively disabling AVX2 on the top 50 modules ranked by centrality results in a substantial reduction in the UF-CAM-ECT failure rate in comparison with AVX2 enabled on all modules. Furthermore, this approach exhibits a substantially lower failure rate than disabling AVX2 on 50 modules at random, and even the top 50 modules by lines of code. See Table 1 for the failure rates. These results indicate that eigenvector centrality accurately captures the information flow between CESM modules and provides a useful ordering. Selective disablement of instructions such as AVX2 balances optimization with preserving statistical consistency and promotes highly efficient CPU usage.

7 CONCLUSIONS AND FUTURE WORK

The goal of this study is to develop methods that make root cause analysis of CESM possible. To this end, we create a toolkit to convert the CESM source code into a digraph together with metadata that represents variable assignment paths and their properties. We note that creating a Python interface for LLVM [22] with Flang [29] would allow our parsing to succeed on any compilable Fortran code. We develop an efficient hybrid static program slicing approach based on combining code coverage with BFS. We combine the Girvan-Newman algorithm with eigenvector in-centrality in series to enable parallel runtime sampling of critical nodes. We perform experiments based on CESM output to demonstrate in simulation how our process can find causes of model discrepancy. Finally, we provide evidence that our methods accurately characterize information flow at runtime by successfully finding variables determined to be susceptible to FMA instructions by a lengthy, manual investigation. Creating a method to identify which variables to sample to re-

fine the root cause search space is a significant accomplishment. However, developing and implementing a sampling procedure for the running model is a challenging undertaking that remains to be done.

The power of the methods developed in this work is derived from the translation of source code into a directed graph representation that enables fast, static analysis of information flow. Graph theory is an expansive field that offers a large number of sophisticated ways to analyze variable relationships. Allowing scientists and engineers to apply these techniques to root cause analysis is a significant achievement. In future work, combining the static directed graph with runtime values into a fully-featured root cause analysis suite for CESM will provide a level of quality assurance not currently available. Modifying our method to enable quality assurance for other codes is future work.

ACKNOWLEDGEMENTS

We wish to thank Dong Ahn, John Dennis, and Sriram Sankaranarayanan for their helpful advice. We are especially grateful to Ganesh Gopalakrishnan, Michael Bentley, and Ian Briggs for thoroughly reading our draft and for their detailed feedback. This research used computing resources provided by the Climate Simulation Laboratory at NCAR's Computational and Information Systems Laboratory (CISL), sponsored by the National Science Foundation and other agencies.

REFERENCES

- [1] ARM. *Allinea Forge*. <https://developer.arm.com/docs/101136/0701/allinea-forge>. Accessed: 2018-08-19. 2018.
- [2] A. H. Baker, D. M. Hammerling, M. N. Levy, H. Xu, J. M. Dennis, B. E. Eaton, J. Edwards, C. Hannay, S. A. Mickelson, R. B. Neale, D. Nychka, J. Shollenberger, J. Tribbia, M. Vertenstein, and D. Williamson. “A new ensemble-based consistency test for the Community Earth System Model”. In: *Geoscientific Model Development* 8 (2015), pp. 2829–2840. doi: 10.5194/gmd-8-2829-2015.
- [3] A. H. Baker, Y. Hu, D. M. Hammerling, Y.-H. Tseng, H. Xu, X. Huang, F. O. Bryan, and G. Yang. “Evaluating statistical consistency in the ocean model component of the Community Earth System Model (pyCECT v2.0)”. In: *Geoscientific Model Development* 9.7 (2016), pp. 2391–2406. doi: 10.5194/gmd-9-2391-2016. URL: <http://www.geosci-model-dev.net/9/2391/2016/>.
- [4] Leeann Bent, Darren C. Atkinson, and William G. Griswold. *A Comparative Study of Two Whole Program Slicers for C*. Tech. rep. La Jolla, CA, USA, 2001.
- [5] Aaron Clauset, Samuel Arbesman, and Daniel B. Larremore. “Systematic inequality and hierarchy in faculty hiring networks”. In: *Science Advances* 1.1 (2015). doi: 10.1126/sciadv.1400005. eprint: <http://advances.sciencemag.org/content/1/1/e1400005.full.pdf>. URL: <http://advances.sciencemag.org/content/1/1/e1400005>.
- [6] Computational And Information Systems Laboratory. *Cheyenne: SGI ICE XA Cluster*. en-us. 2017. doi: 10.5065/d6rx99hx.
- [7] Computational and Information Systems Laboratory. *Yellowstone: IBM iDataPlex System (Climate Simulation Laboratory)*. <http://n2t.net/ark:/85065/d7wd3xhc>. Boulder, CO: National Center for Atmospheric Research, 2016.
- [8] Argonne Leadership Computing Facility. *Mira*. <https://www.alcf.anl.gov/mira>. Accessed: 2018-08-16. 2018.
- [9] Linton C. Freeman. “Centrality in social networks conceptual clarification”. In: *Social Networks* 1.3 (1978), pp. 215–239. ISSN: 0378-8733. doi: [https://doi.org/10.1016/0378-8733\(78\)90021-7](https://doi.org/10.1016/0378-8733(78)90021-7). URL: <http://www.sciencedirect.com/science/article/pii/0378873378900217>.
- [10] M. Girvan and M. E. J. Newman. “Community structure in social and biological networks”. In: *Proceedings of the National Academy of Sciences* 99.12 (2002), pp. 7821–7826. ISSN: 0027-8424. doi: 10.1073/pnas.122653799. eprint: <http://www.pnas.org/content/99/12/7821.full.pdf>. URL: <http://www.pnas.org/content/99/12/7821>.
- [11] Rajiv Gupta and Mary Lou Soffa. “Hybrid Slicing: An Approach for Refining Static Slices Using Dynamic Information”. In: *Proceedings of the 3rd ACM SIGSOFT Symposium on Foundations of Software Engineering*. SIGSOFT '95. Washington, D.C., USA: ACM, 1995, pp. 29–40. ISBN: 0-89791-716-2. doi: 10.1145/222124.222137. URL: <http://doi.acm.org/10.1145/222124.222137>.
- [12] Aric Hagberg, Pieter Swart, and Daniel Schult. “Exploring network structure, dynamics, and function using NetworkX”. In: *Proceedings of the 7th Python in Science Conference (SciPy 2008)*. 2008, pp. 11–15.
- [13] William R. Harris, Sriram Sankaranarayanan, Franjo Ivančić, and Aarti Gupta. “Program Analysis via Satisfiability Modulo Path Programs”. In: *Proceedings of the 37th Annual ACM SIGPLAN-SIGACT Symposium on Principles of Programming Languages*. POPL '10. Madrid, Spain: ACM, 2010, pp. 71–82. ISBN: 978-1-60558-479-9. doi: 10.1145/1706299.1706309. URL: <http://doi.acm.org/10.1145/1706299.1706309>.
- [14] Ki-ichiro Hashimoto and Akira Hori. “Selberg-Ihara's Zeta function for p-adic Discrete Groups”. In: *Automorphic Forms and Geometry of Arithmetic Varieties*. Ed. by K. Hashimoto and Y. Namikawa. Vol. 15. Advanced Studies in Pure Mathematics. Academic Press, 1989, pp. 171–210. ISBN: 978-0-12-330580-0. doi: <https://doi.org/10.1016/B978-0-12-330580-0.50014-8>. URL: <http://www.sciencedirect.com/science/article/pii/B9780123305800500148>.
- [15] Martijn P. van den Heuvel and Olaf Sporns. “Network hubs in the human brain”. In: *Trends in Cognitive Sciences* 17.12 (Dec. 2013), pp. 683–696. ISSN: 1364-6613. doi: 10.1016/j.tics.2013.09.012. URL: <http://dx.doi.org/10.1016/j.tics.2013.09.012>.
- [16] University of Illinois/NCSA. *Clang*. <http://clang.llvm.org/>. Accessed: 2018-08-16. 2007.

- [17] Intel. *Intel Fortran Compiler 17.0 Developer Guide and Reference Code Coverage Tool*. <https://software.intel.com/en-us/node/680224>. Accessed: 2018-01-24. 2017.
- [18] Joxan Jaffar, Vijayaraghavan Murali, Jorge A. Navas, and Andrew E. Santosa. “Path-Sensitive Backward Slicing”. In: *Proceedings of the 19th International Conference on Static Analysis*. SAS’12. Deauville, France: Springer-Verlag, 2012, pp. 231–247. ISBN: 978-3-642-33124-4. DOI: 10.1007/978-3-642-33125-1_17. URL: http://dx.doi.org/10.1007/978-3-642-33125-1_17.
- [19] J. E. Kay, C. Deser, A. Phillips, A. Mai, C. Hannay, G. Strand, J. M. Arblaster, S. C. Bates, G. Danabasoglu, J. Edwards, M. Holland, P. Kushner, J.-F. Lamarque, D. Lawrence, K. Lindsay, A. Middleton, E. Munoz, R. Neale, K. Oleson, L. Polvani, and M. Vertenstein. “The Community Earth System Model (CESM) Large Ensemble Project: A Community Resource for Studying Climate Change in the Presence of Internal Climate Variability”. In: *Bulletin of the American Meteorological Society* 96.8 (2015), pp. 1333–1349. DOI: 10.1175/BAMS-D-13-00255.1. eprint: <http://dx.doi.org/10.1175/BAMS-D-13-00255.1>. URL: <http://dx.doi.org/10.1175/BAMS-D-13-00255.1>.
- [20] Y. Kim, J. M. Dennis, and C. Kerr. “Assessing Representativeness of Kernels Using Descriptive Statistics”. In: *2017 IEEE International Conference on Cluster Computing (CLUSTER)*. Sept. 2017, pp. 818–825. DOI: 10.1109/CLUSTER.2017.117.
- [21] Younsung Kim, John Dennis, Christopher Kerr, Raghu Raj Parasanna Kumar, Amogh Simha, Allison Baker, and Sheri Mickelson. “KGEN: A Python Tool for Automated Fortran Kernel Generation and Verification”. In: *Procedia Computer Science*. Vol. 80. ICCS 2016. The International Conference on Computational Science. 2016, pp. 1450–1460. DOI: 10.1016/j.procs.2016.05.466.
- [22] Chris Lattner and Vikram Adve. “LLVM: A Compilation Framework for Lifelong Program Analysis & Transformation”. In: *Proceedings of the International Symposium on Code Generation and Optimization: Feedback-directed and Runtime Optimization*. CGO ’04. Palo Alto, California: IEEE Computer Society, 2004, pp. 75–. ISBN: 0-7695-2102-9. URL: <http://dl.acm.org/citation.cfm?id=977395.977673>.
- [23] Travis Martin, Xiao Zhang, and M. E. J. Newman. “Localization and centrality in networks”. In: *Phys. Rev. E* 90 (5 Nov. 2014), p. 052808. DOI: 10.1103/PhysRevE.90.052808. URL: <https://link.aps.org/doi/10.1103/PhysRevE.90.052808>.
- [24] D. J. Milroy, A. H. Baker, D. M. Hammerling, and E. R. Jessup. “Nine time steps: ultra-fast statistical consistency testing of the Community Earth System Model (pyCECT v3.0)”. In: *Geoscientific Model Development* 11.2 (2018), pp. 697–711. DOI: 10.5194/gmd-11-697-2018. URL: <https://www.geosci-model-dev.net/11/697/2018/>.
- [25] Daniel J. Milroy, Allison H. Baker, Dorit M. Hammerling, John M. Dennis, Sheri A. Mickelson, and Elizabeth R. Jessup. “Towards Characterizing the Variability of Statistically Consistent Community Earth System Model Simulations”. In: *Procedia Computer Science* 80. Supplement C (2016). International Conference on Computational Science 2016, ICCS 2016, 6-8 June 2016, San Diego, California, USA, pp. 1589–1600. ISSN: 1877-0509. DOI: <https://doi.org/10.1016/j.procs.2016.05.489>. URL: <http://www.sciencedirect.com/science/article/pii/S1877050916309759>.
- [26] M. E. J. Newman and M. Girvan. “Finding and evaluating community structure in networks”. In: *Phys. Rev. E* 69 (2 Feb. 2004), p. 026113. DOI: 10.1103/PhysRevE.69.026113. URL: <https://link.aps.org/doi/10.1103/PhysRevE.69.026113>.
- [27] Lawrence Page, Sergey Brin, Rajeev Motwani, and Terry Winograd. *The PageRank Citation Ranking: Bringing Order to the Web*. Technical Report 1999-66. Previous number = SIDL-WP-1999-0120. Stanford InfoLab, Nov. 1999. URL: <http://ilpubs.stanford.edu:8090/422/>.
- [28] Pearu Peterson. “F2PY: a tool for connecting Fortran and Python programs”. In: *International Journal of Computational Science and Engineering* 4.4 (2009), pp. 296–305. DOI: 10.1504/IJCSE.2009.029165. URL: <https://www.inderscienceonline.com/doi/abs/10.1504/IJCSE.2009.029165>.
- [29] PGI. *Flang*. <https://github.com/flang-compiler/flang>. Accessed: 2018-08-14. 2017.
- [30] Marcel Salathé, Maria Kazandjieva, Jung Woo Lee, Philip Levis, Marcus W. Feldman, and James H. Jones. “A high-resolution human contact network for infectious disease transmission”. In: *Proc Natl Acad Sci USA* 107.51 (Dec. 2010). 21149721[pmid], pp. 22020–22025. ISSN: 0027-8424. DOI: 10.1073/pnas.1009094108. URL: <http://www.ncbi.nlm.nih.gov/pmc/articles/PMC3009790/>.
- [31] G. Sawaya, M. Bentley, I. Briggs, G. Gopalakrishnan, and D. H. Ahn. “FLIT: Cross-platform floating-point result-consistency tester and workload”. In: *2017 IEEE International Symposium on Workload Characterization (IISWC)*. Oct. 2017, pp. 229–238. DOI: 10.1109/IISWC.2017.8167780.
- [32] Devavrat Shah and Tauhid Zaman. “Detecting Sources of Computer Viruses in Networks: Theory and Experiment”. In: *SIGMETRICS Perform. Eval. Rev.* 38.1 (June 2010), pp. 203–214. ISSN: 0163-5999. DOI: 10.1145/1811099.1811063. URL: <http://doi.acm.org/10.1145/1811099.1811063>.
- [33] Sameer S. Shende and Allen D. Malony. “The Tau Parallel Performance System”. In: *Int. J. High Perform. Comput. Appl.* 20.2 (May 2006), pp. 287–311. ISSN: 1094-3420. DOI: 10.1177/1094342006064482. URL: <http://dx.doi.org/10.1177/1094342006064482>.
- [34] Josep Silva. “A Vocabulary of Program Slicing-based Techniques”. In: *ACM Comput. Surv.* 44.3 (June 2012), 12:1–12:41. ISSN: 0360-0300. DOI: 10.1145/2187671.2187674. URL: <http://doi.acm.org/10.1145/2187671.2187674>.
- [35] RogueWave Software. *TotalView*. <https://support.roguewave.com/documentation/tvdocs/en/2018/>. Accessed: 2018-08-19. 2018.

- [36] Frank Tip. *A Survey of Program Slicing Techniques*. Tech. rep. Amsterdam, The Netherlands, The Netherlands, 1994.
- [37] M. Weiser. “Program Slicing”. In: *IEEE Transactions on Software Engineering* SE-10.4 (July 1984), pp. 352–357. issn: 0098-5589. doi: 10.1109/TSE.1984.5010248.
- [38] Mark Weiser. “Program Slicing”. In: *Proceedings of the 5th International Conference on Software Engineering*. ICSE '81. San Diego, California, USA: IEEE Press, 1981, pp. 439–449. isbn: 0-89791-146-6. url: <http://dl.acm.org/citation.cfm?id=800078.802557>.

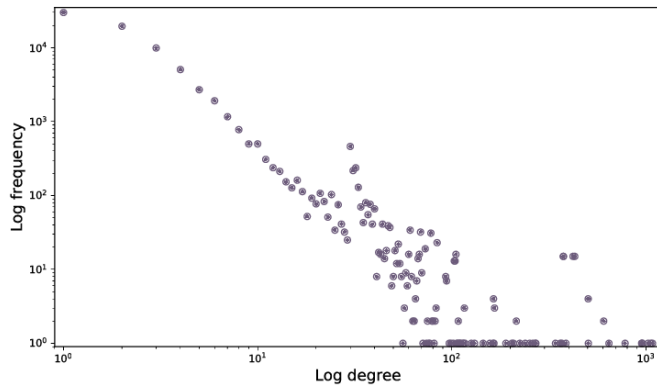


Figure 9: Degree distribution of nodes in the CESM digraph.

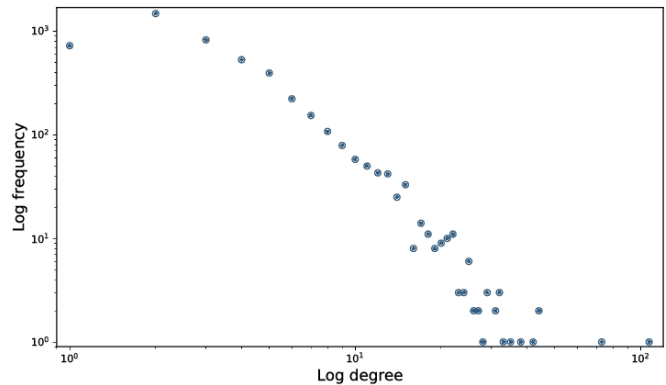


Figure 10: Degree distribution of nodes in the GOFFGRATCH digraph.

8 SUPPLEMENTARY MATERIAL

8.1 Hashimoto non-backtracking centrality

Scale-free or power law graphs which have degree distributions that are negative exponentials with exponent magnitude greater than 2.5 are identified as causing localization in [23]. The degree distribution of the total CESM graph approximately follows a power law, as can be seen in Figure 9. Induced subgraphs of the CESM graph are also approximately scale-free, consistent with the properties of such graphs (see Figure 10 for the GOFFGRATCH experiment subgraph). A natural question is whether the concentration of centrality on graph hubs has undesirable effects on the ranking of nodes. The application of non-backtracking or Hashimoto centrality [14] as a substitute for eigenvector centrality for power law graphs is discussed in [23]. We compare the two centralities in Figure 11 for the GOFFGRATCH experiment. The Hashimoto non-backtracking centrality indeed distributes the centrality from the hubs to other nodes, but the effect is subtle until approximately the 300th ranked node. Also note that the Hashimoto centrality does not provide a rank for all nodes in the subgraph, as can be noted by the sharp drop at the end of its curve in Figure 11. This is due to the Hashimoto centrality's use of the line graph of the subgraph's adjacency matrix, which excludes nodes with no neighbors. Although we determine that the non-backtracking centrality provides at best marginal improvement over eigenvector centrality for our graph, we provide a derivation based on that which appears in [23]. Hashimoto centrality may prove beneficial for models with graphs that follow power laws that produce more pronounced localization [23].

8.1.1 Centrality derivation

This section is a reformulation of the derivation in [23], which we have reworked in the interest of clarity. Let G be a graph with $n \times n$ adjacency matrix \mathbf{A} , set of nodes V and edges E . The graph order is the number of nodes: $|V| = n$, while the graph size is the number of edges: $|E| = m$. Note that m is the number of nonzero entries in \mathbf{A} if G is directed, and the number of nonzero entries in the upper or lower triangle of \mathbf{A} if G is undirected.

Let $e \in E$ be represented as (v_1, v_2) . If G is directed, $(v_1, v_2) \neq (v_2, v_1)$ and the order represents direction: $v_1 \rightarrow v_2 := (v_1, v_2)$. If G is undirected, $(v_1, v_2) = (v_2, v_1)$.

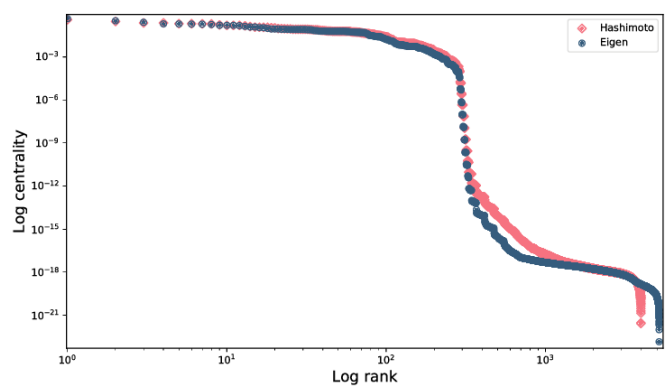


Figure 11: Log rank versus log absolute value of centrality for Hashimoto non-backtracking centrality and eigenvector centrality in the GOFFGRATCH experiment subgraph. The absolute value of the centralities is used since the lowest ranked terms are small negative numbers.

Let $N(i)$ be the set of neighbors of node i .

The Hashimoto, or non-backtracking matrix [14] of graph G is denoted \mathbf{B} and is an adjacency matrix on E :

$$\forall (u, v), (w, x) \in E;$$

$$B_{(u,v),(w,x)} \text{ or } B_{(u \rightarrow v),(w \rightarrow x)} = \delta_{vw}(1 - \delta_{ux})$$

Where δ is the Kronecker delta. For an undirected graph, each $(v_1, v_2) \in E$ becomes two ordered pairs $(v_1, v_2), (v_2, v_1)$. Thus \mathbf{B} is $m \times m$ if G is directed, and $2m \times 2m$ for undirected G . \mathbf{B} is closely related to the *line graph* $L(G)$ which is also an adjacency matrix on E : $L(G)_{(u \rightarrow v),(w \rightarrow x)} := \delta_{vw}$

Instead of computing the eigenvector centrality on \mathbf{A} , we use \mathbf{B} . Let λ be the Perron-Frobenius (leading) eigenvalue of \mathbf{B} , and \vec{v} be the corresponding eigenvector. Then the out-centrality (corresponding to out-edges) for some $i \in V$ can be derived by starting from the eigenvector equation $\lambda \vec{v} = \mathbf{B} \vec{v}$. To compute the in-centrality used in this work, we can reverse the directed edges of \mathbf{A} (via the transpose \mathbf{A}^T).

$$\begin{aligned}
\vec{v}_{(i \rightarrow j)} &= \frac{1}{\lambda} \sum_{(k \rightarrow l) \in N((i \rightarrow j))} B_{(i \rightarrow j), (k \rightarrow l)} \vec{v}_{(k \rightarrow l)} \\
&= \frac{1}{\lambda} \sum_{(k \rightarrow l) \in N((i \rightarrow j))} \delta_{jk} (1 - \delta_{il}) \vec{v}_{(k \rightarrow l)} \\
&= \frac{1}{\lambda} \sum_k^n \sum_l^n A_{kl} \delta_{jk} (1 - \delta_{il}) \vec{v}_{(k \rightarrow l)} \\
&= \frac{1}{\lambda} \sum_l^n A_{jl} (1 - \delta_{il}) \vec{v}_{(j \rightarrow l)}
\end{aligned}$$

or

$$\vec{v}_{(i \rightarrow j)} = \frac{1}{\lambda} \sum_{l \neq i}^n A_{jl} \vec{v}_{(j \rightarrow l)}$$

then the full non-backtracking centrality of node i is:

$$c_i = \sum_{q \in N(i)} \vec{v}_{(i \rightarrow q)}$$

Where we are free to choose a constant to normalize the centrality.

8.2 Additional experimental results

As in Section 6 we omit communities of fewer than four nodes in the interest of plot clarity. Note that we refer to the Girvan-Newman algorithm ([10, 26]) as G-N.

8.2.1 RANDBUG

We select the module for this bug by randomly choosing a module from the set of CAM modules known to be executed by our simulation in the first time step. We introduce an error in the array index of a variable used to assign the contents of the derived type containing physics state variables (t, u, v, etc.), in particular the state variable omega. As in the previous experiment, this change results in a UF-CAM-ECT failure. Omega is output to file with the value `state%omega`, so we use “omega” as the canonical name for generating the induced subgraph. This experiment is more challenging than WSUBBUG, as omega is computed in other CAM modules, yielding a subgraph of 628 nodes and 295 edges. Applying the G-N algorithm to the remaining nodes identifies several small (fewer than 30 nodes) communities, one of whose most central node is the bug source. See Figure 12.

8.2.2 DYN3BUG

Another example of a bug consisting of a single line change is located in a dynamics subroutine that computes hydrostatic pressure in the CAM core. The bug particularly affects the five variables listed in Table 2. We apply our iterative refinement to the induced subgraph of 5,999 nodes and 11,495 edges (Figure 13a), and successfully separate the orange dynamics community from the blue physics community. Instrumenting the light blue,

most central nodes in Figure 13c would detect a difference in values between ensemble and experimental runs, as at least one instrumented node is reachable from the bug. Inducing a subgraph on nodes contained in paths terminating on the central nodes connected to the bug further reduces the size of the subgraph. The second iteration of the refinement procedure yields a subgraph identical to Figure 14a, so further refinement will not be possible without analysis of true runtime values.

8.2.3 AVX2

Figure 15 is an assertion that restricting our induced subgraph nodes to variables present in CAM is not necessary for finding the sources of inconsistency (but it does reduce the number of algorithm 5.4 iterations for plotting purposes). This subgraph is created with the same affected variable list as Figure 8, but allows nodes outside of CAM (such as in the land model). Although the graph is larger (7,796 nodes and 16,532 edges), it manifests the community structure of the CAM core (purple cluster). The second iteration of algorithm 5.4 reveals a community that is very similar to the AVX2 subgraph in Section 6.4. The nodes with the largest centralities in the community are the same as those in Figure 8a. This suggests that the same conclusions are reached with this subgraph after a single additional of iteration.

Table 2: CAM output variables selected by the methods described in paper Section 3, and their internal counterparts.

Experiment	Output variables	Internal variables
WSUBBUG	wsub	wsub
RANDBUG	omega	omega
GOFFGRATCH	aqsnow, freqs, cldhgh, precsl, ansnow, cldmed, cloud, cldlow, ccn3, cldtot	qsout2, freqs, clhgh, snowl, nsout2, clmed, cld, cldlow, ccn, cltot
DYN3BUG	vv, omega, z3, uu, omegat	v, omega, z3, u, t
RAND-MT	flds, taux, snowhnd, flns, qrl	flwds, wsx, snowhland, flns, qrl
AVX2	taux, trefht, snowhnd, ps, u10, shflx	wsx, tref, snowhland, ps, u10, shf

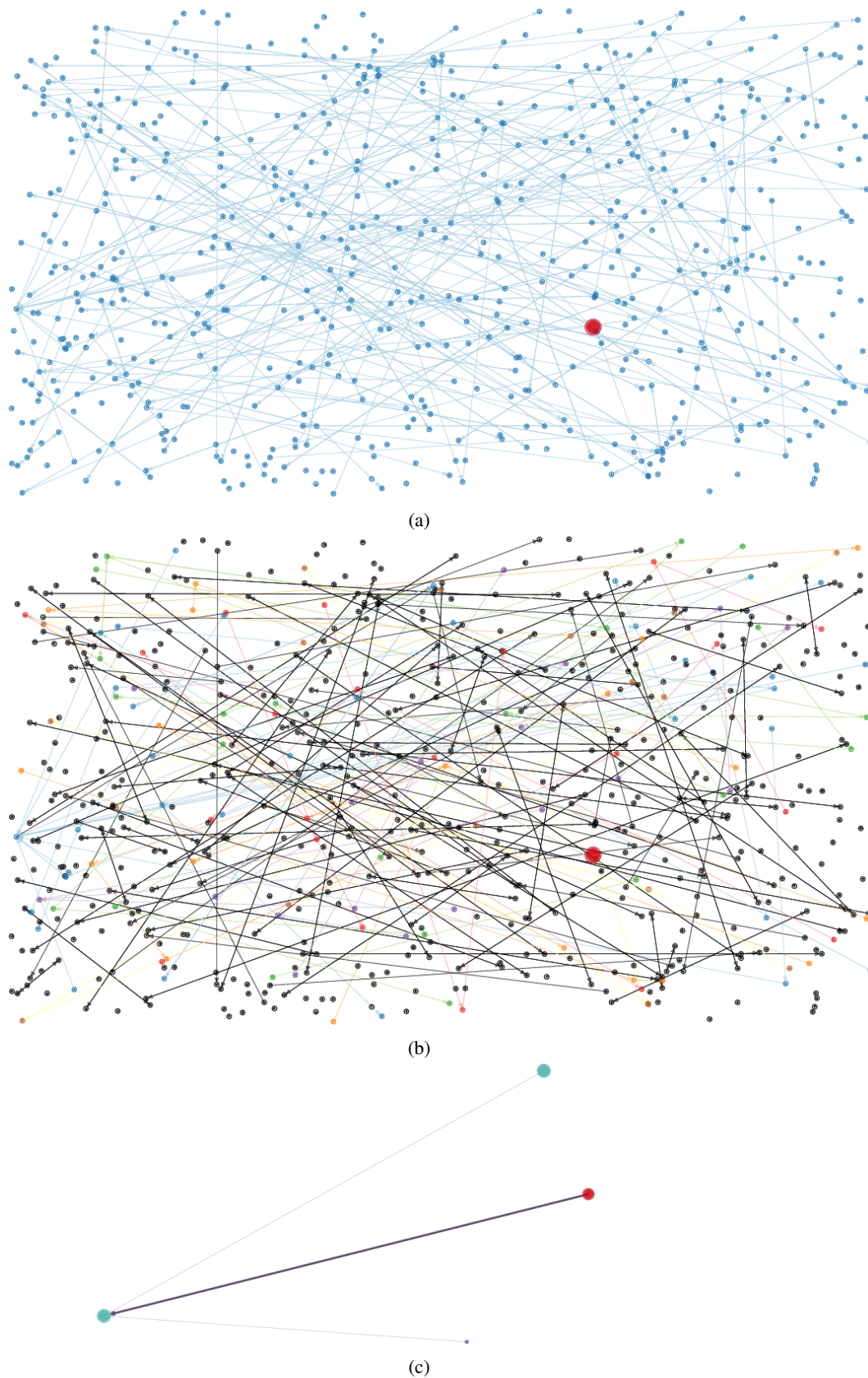


Figure 12: RANDOMBUG, single iteration. The bug location is indicated by a large red node. In **c**, the light blue nodes are the most central of the small community shown, and the purple edge designates the connection from the bug to the instrumented node.

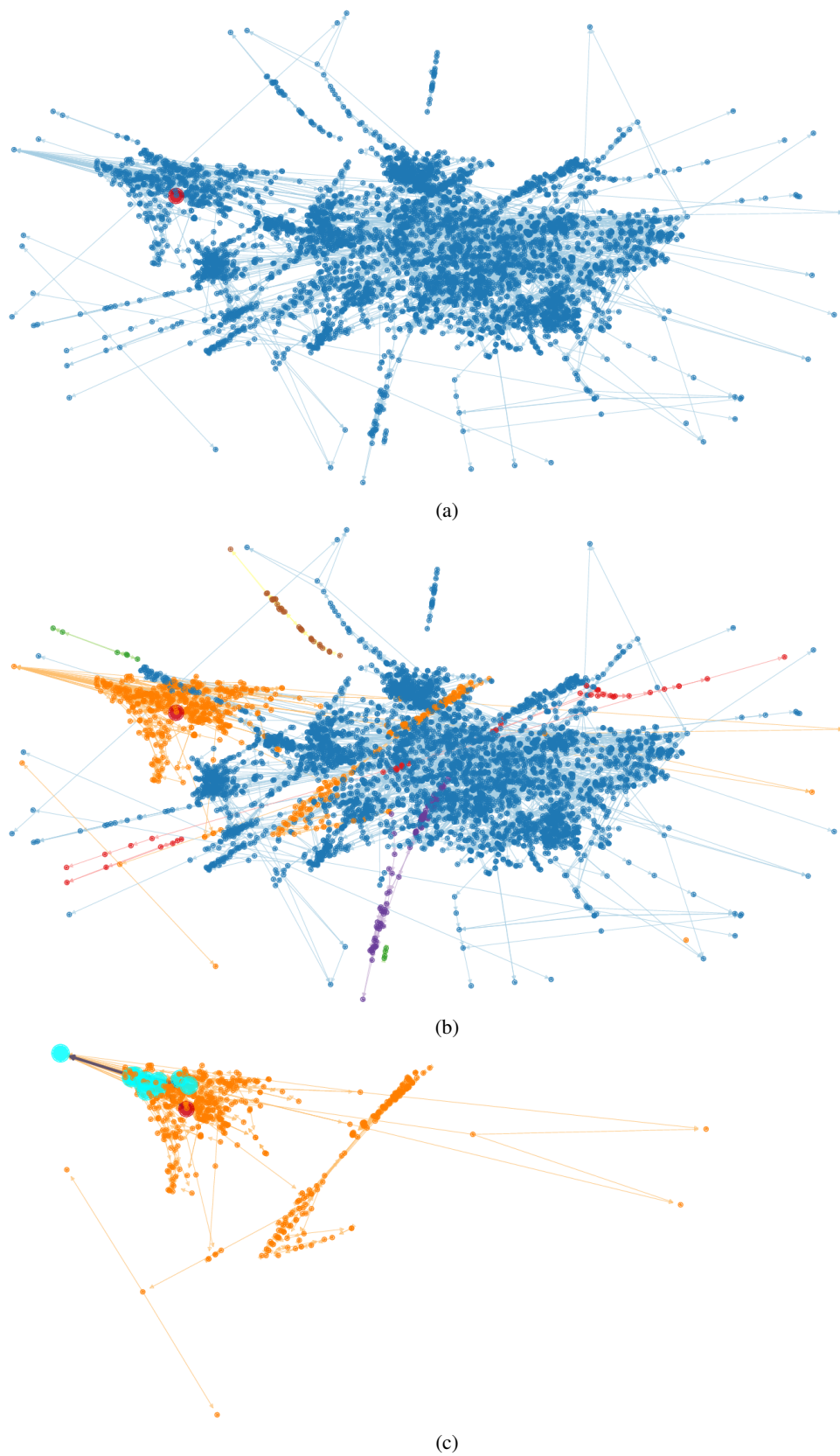
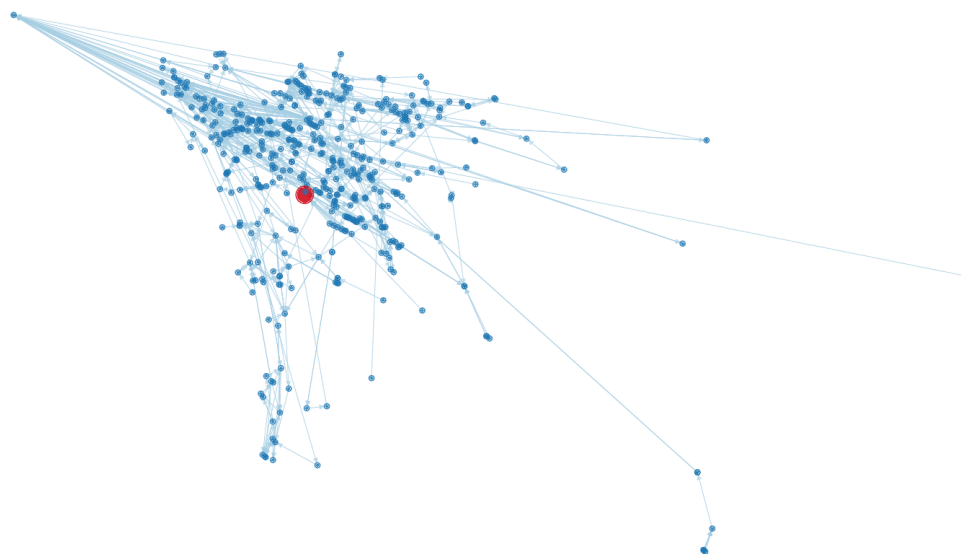
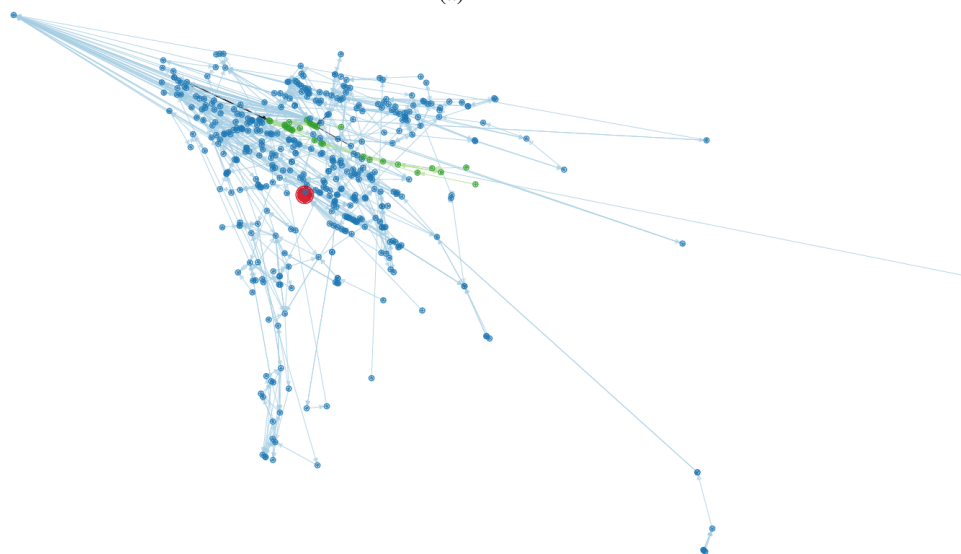


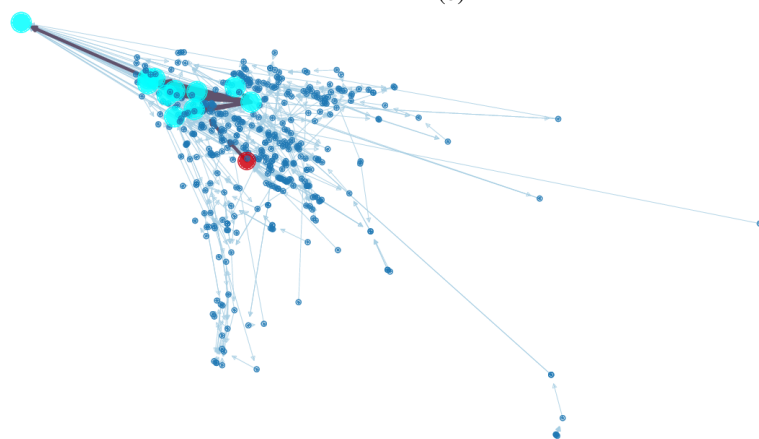
Figure 13: DYN3BUG first iteration. In these figures, the large red node is the bug, and the large, light blue nodes designate the most central nodes to be sampled.



(a)



(b)



(c)

Figure 14: DYN3BUG second iteration. In these figures, the large red node is the bug, and the large, light blue nodes designate the most central nodes to be sampled.

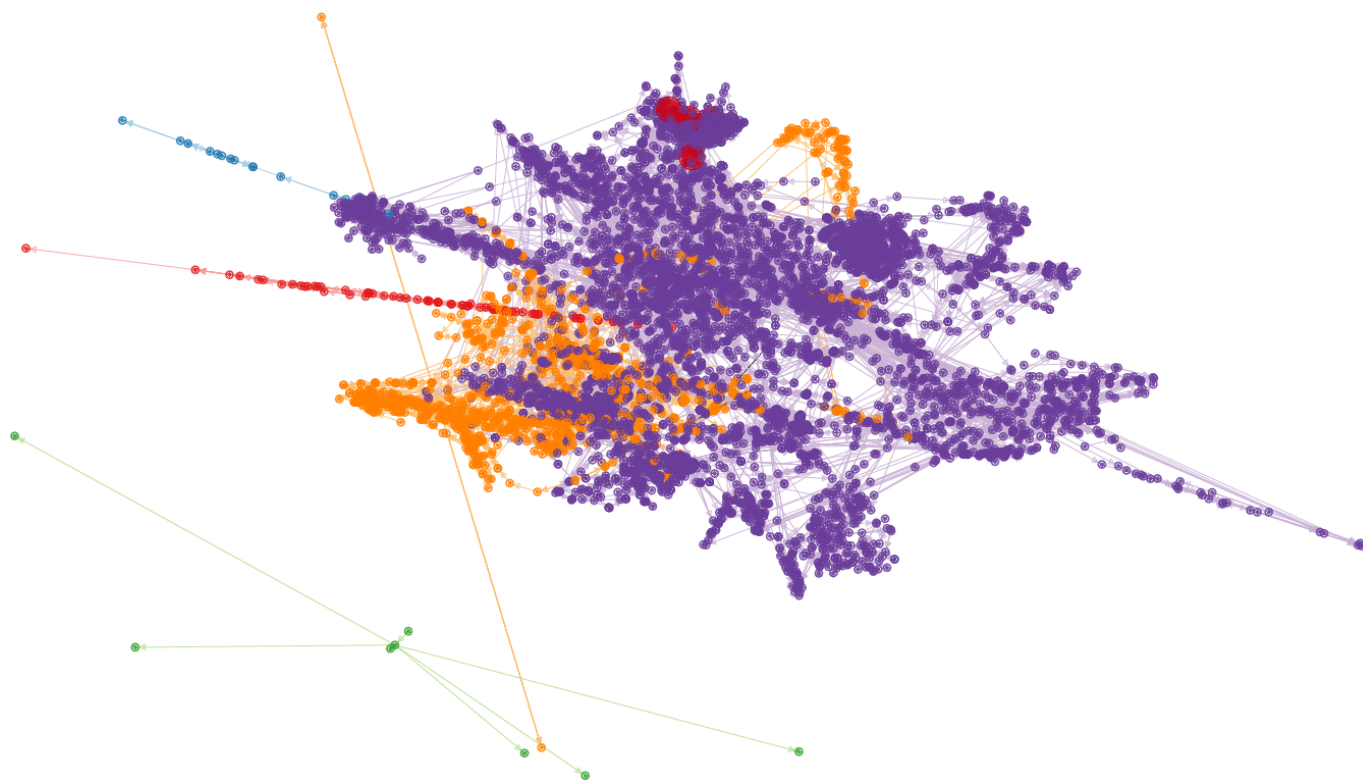


Figure 15: Communities generated by the induced subgraph defined by variables affected by the AVX2 experiment. Variable locations are not restricted to CAM. The variables identified by KGen are colored red.